Available online at www.sciencedirect.com
ScienceDirect
Journal of the Mechanics and Physics of Solids
55 (2007) 2300–2327

JOURNAL OF THE MECHANICS AND PHYSICS OF SOLIDS

www.elsevier.com/locate/jmps

Dislocation nucleation from bicrystal interfaces and grain boundary ledges: Relationship to nanocrystalline deformation

L. Capolungo[a,c,*], D.E. Spearot[b], M. Cherkaoui[a,c], D.L. McDowell[a,c,d], J. Qu[a,c], K.I. Jacob[c,e]

[a]*UMI 2958, Georgia Tech-CNRS, Metz, France*
[b]*Department of Mechanical Engineering, University of Arkansas, Fayetteville, AR 72701, USA*
[c]*G.W. Woodruff School of Mechanical Engineering, France*
[d]*School of Materials Science and Engineering, Georgia Institute of Technology, Atlanta, GA 30332, USA*
[e]*Polymer, Textile and Fiber Engineering, Georgia Institute of Technology, Atlanta, GA 30332, USA*

Received 25 October 2006; received in revised form 27 March 2007; accepted 1 April 2007

Abstract

Molecular dynamics simulations are used to evaluate the primary interface dislocation sources and to estimate both the free enthalpy of activation and the critical emission stress associated with the interfacial dislocation emission mechanism. Simulations are performed on copper to study tensile failure of a planar $\Sigma 5$ $\{2\,1\,0\}$ 53.1° interface and an interface with the same misorientation that contains a ledge. Simulations reveal that grain boundary ledges are more favorable as dislocation sources than planar regions of the interface and that their role is not limited to that of simple dislocation donors. The parameters extracted from the simulations are utilized in a two-phase composite mesoscopic model for nanocrystalline deformation that includes the effects of both dislocation emission and dislocation absorption mechanisms. A self-consistent approach based on the Eshelby solution for grains as ellipsoidal inclusions is augmented by introduction of stress concentration in the constitutive law of the matrix phase to account for more realistic grain boundary effects. Model simulations suggest that stress concentration is required in the standard continuum theory to activate the coupled grain boundary dislocation emission and

*Corresponding author. G.W. Woodruff School of Mechanical Engineering, France. Tel.: +33 387203923.
E-mail address: laurent.capolungo@georgiatech-metz.fr (L. Capolungo).

0022-5096/$ - see front matter © 2007 Elsevier Ltd. All rights reserved.
doi:10.1016/j.jmps.2007.04.001

absorption mechanisms when activation energy of the dislocation source is determined from atomistic calculation on grain boundaries without consideration of impurities or other extrinsic defects.
© 2007 Elsevier Ltd. All rights reserved.

Keywords: Molecular dynamics; Micromechanics; Thermal activation; Nanocrystalline materials; Dislocations

1. Introduction

Identification of the fundamental phenomena responsible for the 'abnormal' mechanical behavior of nanocrystalline (NC) materials is a challenging problem that requires the use of multiple approaches (e.g., molecular dynamics (MD) and micromechanics). In coarse grain polycrystalline materials, the yield strength is proportional to the inverse of the square root of the grain size as given by the Hall–Petch law (Hall, 1951; Petch, 1953). The proportionality coefficient is referred to as the Hall–Petch slope. However, in the case of NC materials, experiments have shown an inverse Hall–Petch slope, i.e., the yield stress decreases for decreasing grain size below a critical grain diameter (Sanders et al.,1997a; Schuh et al., 2002). This phenomenon was also revealed via MD simulations (Wolf et al., 2003; Yamakov et al., 2003). This inverse Hall–Petch slope is one of the characteristics of the 'abnormal' behavior of NC materials.

Also, recent experiments (Wang and Ma, 2004; Lu et al., 2005) revealed that, in the case of face-centered cubic (FCC) NC materials, a decrease in the grain size engenders an increase in the strain rate sensitivity. Recently, Asaro and Suresh (2005) successfully modeled, via a continuum dislocation approach at the microscopic scale, the size effect in the strain rate sensitivity in terms of the decrease of activation volume for dislocation nucleation with grain size. This effect was also investigated via a micromechanical scheme based on fast Fourier transform (Lebensohn et al., 2007).

Although experimental observations and MD simulations suggest the activity of local mechanisms (e.g., Coble creep, twinning, grain boundary dislocation emission, grain boundary sliding), it is rarely possible to directly relate their individual contributions to the macroscopic response of the material. This is primarily due to the fact that the scale and boundary conditions involved in molecular simulations are several orders of magnitude different from that in real experiments. In addition, prior to predicting the global effect of a local phenomenon, a scale transition from the atomic scale to the mesoscopic scale must first be performed, followed by a second scale transition from the mesoscopic scale to the macroscopic scale. Micromechanical schemes have been used in previous models and have proven to be an effective way to perform the second scale transition (Jiang and Weng, 2004; Capolungo et al., 2005a, b). However, as shown in the present study, traditional Eshelbian micromechanical schemes require augmentation to account for localized stress and strain heterogeneities in the constituents. Furthermore, the scale transition from the atomistic scale to the mesoscopic scale is also a critical and complex issue.

The major challenges and recent advances related to multiscale modeling were discussed by Dimiduk et al. (2006). In particular, it is recalled that while predictions of crystallographic textures in metals via coarse graining techniques have been successful, in the case of size-dependent materials, scale transition methods have not yet reached the same level of success. However, as presented by Rickman and LeSar (2006), recent work

based on non-local approaches (Arsenlis et al., 2004) and extensions of the continuous theory of dislocations (LeSar and Rickmann, 2004) are promising techniques to perform the scale transition from the dislocation regime, referred to in this article as the mesoscale, and the macroscopic scale. In particular, the theory of LeSar and Rickman (2004) provides a parametric description of the space and time dependent interaction energies of cells composing the volume of interest. As shown in the present study, statistical mechanics offers a route to perform the transition from the atomic scale to the mesoscopic scale.

The viscoplastic behavior of NC materials has been subject to numerous investigations, most of which are focused on the role of interfaces (grain boundaries and triple junctions) and aimed at identifying the mechanisms responsible for the breakdown of the Hall–Petch relation. However, the nature of the softening mechanism active in grain boundaries is still an issue of research (Konstantinidis and Aifantis, 1998; Cai et al., 2000, 2001; Kumar et al., 2003; Kim and Estrin, 2005). For NC materials with grain sizes ranging from $\sim$100 nm down to $\sim$10 nm, theoretical models, molecular simulations and experiments suggest a transition from dislocation glide dominated deformation, where grain boundaries act primarily as a barrier to dislocation motion, to grain boundary mediated deformation in which three mechanisms have been discussed in the literature.

First, the softening behavior of NC materials may be attributed to the contribution of creep phenomena, such as Coble (1963) creep, accounting for steady state vacancy diffusion along the grain boundaries (Coble, 1963; Sanders et al., 1997b; Kim et al., 2000, 2001, 2005). This hypothesis is motivated by several experimental observations and models which revealed that creep mechanisms could operate at room temperature in the quasistatic regime (Yin et al., 2001). Also, MD simulations on NC Pd at elevated temperature showed the activity of diffusion mechanism similar to Coble creep under the application of high tensile stresses (Yamakov et al., 2002). However, more recent work has suggested that the observation of creep phenomena could also be due to the presence of flaws in the initial structure of the samples, e.g., presence of porosity at nanoscales (Li et al., 2004).

Second, both MD simulations (Warner et al., 2006) and experimental studies (Ke et al., 1995) have shown that solid motion of grains (e.g., grain boundary sliding or grain rotation) is one of the primary plastic deformation mechanisms in NC materials. For example, MD simulations on shear of bicrystal interfaces (Warner et al., 2006) showed that grain boundary sliding could be appropriately characterized as a stick-slip mechanism. Moreover, grain boundary sliding could operate simultaneously with interface dislocation emission (Kumar et al., 2003; Wang et al., 2005). Discussion in the literature has focused on the possible accommodation of these mechanisms by vacancy diffusion (Van Swygenhoven and Caro, 1997; Kumar et al., 2003). For example, ex situ TEM observations of electrodeposited nickel (Kumar et al., 2003) clearly show the creation of cracks localized at grain boundaries. Recently, an interface separation criterion was introduced to predict the observed low ductility of NC materials with small grain sizes ($<\sim$50 nm) (Wei and Anand, 2004). The authors indicated that a detailed description of the dislocation emission mechanism could improve their model predictions.

Third, MD simulations on 2D columnar structures (Yamakov et al., 2001), 3D NC samples (Derlet and Van Swygenhoven, 2002) and planar bicrystal interfaces (Sansoz and Molinari, 2005; Spearot et al., 2005, 2007) suggest that interfacial dislocation emission can play a prominent role in NC material deformation (Yamakov et al., 2001; Van Swygenhoven et al., 2004). The grain boundary dislocation emission mechanism was first

suggested by Li (1963) in order to describe the Hall–Petch relation. In this model, dislocations are emitted by grain boundary ledges which act as simple dislocation donors in the sense that a ledge can emit a limited number of dislocations equal to the number of extra atomic planes associated with the height of the ledge. Once the dislocation source is exhausted, the ledge is annihilated and the interface becomes defect free. Recent work has indicated that planar interfaces (without ledges or steps) can also emit dislocations, as exhibited by models based on energy considerations (Gutkin et al., 2003) and atomistic simulations on bicrystal interfaces (Sansoz and Molinari, 2005; Spearot et al., 2005, 2007). Moreover, MD simulations of 2D columnar and 3D NC geometries lead to similar conclusions regarding the role of the interface on dislocation emission (Yamakov et al., 2001; Van Swygenhoven et al., 2004). The latter have also shown that grain boundary dislocation emission is a thermally activated mechanism, although there are differences in the definition of the criterion for emission of the trailing partial dislocations. A mesoscopic model accounting for the effect of thermally activated grain boundary dislocation emission and absorption has recently been developed and shows that the breakdown of the Hall–Petch relation could be a consequence of the absorption of dislocations emitted by grain boundaries (Capolungo et al., 2007). The model also raises the question of the identification of the primary interface dislocation emission sources (e.g., boundary segment or ledge).

As discussed in the work of Asaro et al. (2003), who evaluated the stability of dislocations nucleated from grain boundaries using energetic considerations, a crossover from grain boundary dislocation emission to grain boundary sliding occurs at a critical grain size directly related to the stacking fault energy and strain rate. For example, in the case of copper at low strain rates ($\sim 5 \times 10^{-5}\,\mathrm{s}^{-1}$) the critical grain size at which this transition occurs is on the order of $\sim$30 nm, while at higher strain rates ($> 10^{-3}\,\mathrm{s}^{-1}$) the transition would not occur.

Analogous to grain boundary mediated mechanisms, dislocation activity within the grain interiors is also size dependent. Specifically, the initial dislocation density within grain interiors of NC materials is known to decrease with grain size, although experiments are sorely needed to incorporate such size dependent densities in continuum based models. Available experimental data on 30 nm NC Ni suggests that at this particular grain size, grain interiors are virtually dislocation free (Kumar et al., 2003). In addition, due to the fabrication process, deformation twins are sometimes observed within the crystallites (Zhu and Langdon, 2005) which will reduce the mean free path of emitted dislocations and may serve as dislocation barriers. Recent MD simulations on 12 nm NC Al showed that twin boundaries can also act as dislocation sources, facilitating dislocation activity (Froseth et al., 2006).

In this paper, a framework enabling the scale transition from the atomistic scale to the macroscopic scale is developed and used to predict the effect of grain boundary dislocation emission on the response of pure FCC NC materials as well as to identify the primary dislocation sources (e.g., disclinations, ledges). The influence of grain boundary sliding is not modeled in this approach and is subject to ongoing studies in which a generalized secant self-consistent scheme will be developed. The methodology is described in Fig. 1. First, a statistically representative volume element (RVE) composed of grain interiors, grain boundaries and triple junctions is chosen. The RVE is constituted as a two-phase composite material composed of an inclusion phase representing grain interiors and a matrix phase which represents both grain boundaries and triple junctions.

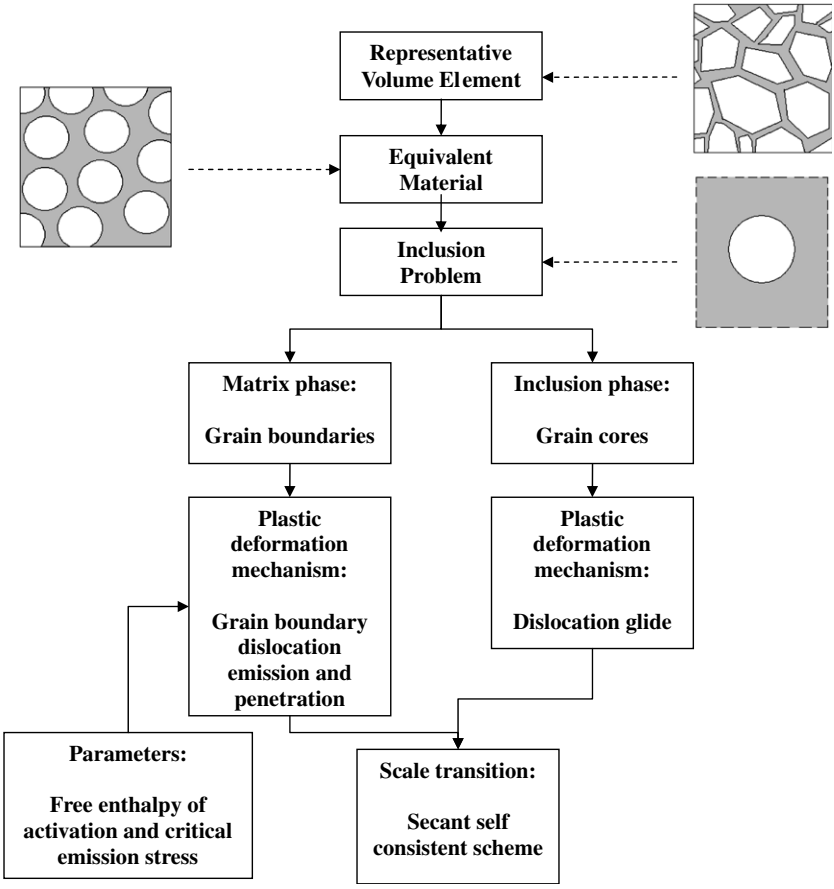

Fig. 1. Schematic of the hierarchical scale transition method.

The behavior of the inclusion phase is governed by dislocation glide which is described with a power law relation. The behavior of the matrix phase is given by a recently introduced constitutive law, presented in Section 2, accounting for the combined effect of grain boundary dislocation emission and absorption (Capolungo et al., 2007). The constitutive law describing the behavior of the matrix phase necessitates the estimation of the free enthalpy of activation and the critical emission stress which are approximated via MD simulations of dislocation nucleation from planar and stepped interfaces, presented in Section 3. A comparison of results in the case of planar and stepped interfaces will also lead to the identification of the principal grain boundary dislocation sources.

Let us note here that similar approaches, enabling a scale transition from the atomistic to the mesoscopic, were successfully developed and applied to the case of thin films (Haslam et al., 2002; Buehler et al., 2003, 2004). Recently a novel method based on the coupling of the material point method and of MD was introduced to simulate the response of a single silicon crystal in tension (Lu et al., 2006).

Traditionally, when using Eshelbian micromechanical schemes the equivalent problem leads to the solution of the inclusion problem in which an inclusion is embedded in a

matrix of infinite dimensions. The solution of this problem will ensure the scale transition from the mesoscopic scale to the macroscopic scale, as presented in Section 4. Note that the predicted behaviors shall be considered as estimates of the actual behavior since the stress and strain fields are assumed to be homogeneous in both the inclusion and the matrix phases.

2. Model for grain boundary dislocation emission and absorption mechanisms

In this section, the mechanism describing the behavior of the matrix phase, representing both grain boundaries and triple junctions, is presented. As stated above, the effect of grain boundary sliding is not considered in the present study; only the effect of grain boundary dislocation emission and absorption is considered. A modification of a previously developed model by the authors, accounting for the grain boundary emission and absorption mechanisms (Capolungo et al., 2007), is introduced to account for the effect of stress concentrations at grain boundaries.

As discussed in the continuum study by Asaro and Suresh (2005), during local sliding events, stress concentrations on the order of 20% can occur at grain boundaries. Recent finite element simulations have suggested much higher stress concentrations (factor of two or three) at triple junctions (Benkassem et al., 2007), although these predictions may overestimate concentration due to the simplicity of the geometry and neglect of actual boundary structure.

In the NC regime, where interfacial dislocation emission is expected to operate, grain interiors are essentially defect free (Kumar et al., 2003). Hence, a dislocation emitted from a grain boundary has a high probability to end its trajectory by absorption into the grain boundary opposite the emission site, leading to mass transfer within the matrix phase. This mass transfer could act has an accommodation process to grain boundary sliding. Neither MD simulations nor TEM experiments have suggested that the emission event leads to long distance mass transfer in the neighborhood of the dislocation source; thus, it is assumed that the emission event does not directly lead to a net strain localized at the emission site. As a first approximation, the thermally activated dislocation emission event can be considered as the trigger to the absorption event, with the absorption event leading to a net strain within the matrix phase. This simple description will clearly over predict the effect of grain boundary dislocation absorption as experimental studies have shown an increase in the stacking fault density in NC Pd during cold rolling, suggesting imperfect dislocation activity within the grain interiors (Markmann et al., 2003). A more complete description of the dislocation emission and absorption mechanisms would include a criterion defining the probability of storage of an emitted dislocation which cannot be based on traditional strain hardening theories since grain interiors are dislocation free when interfacial dislocation emission operates.

Locally in the matrix phase, the average equivalent viscoplastic strain rate engendered by thermally activated grain boundary dislocation emission, noted $\dot{\varepsilon}_{\mathrm{eq}}^{\mathrm{M,vp}}$, is written as

$$\dot{\varepsilon}_{\mathrm{eq}}^{\mathrm{M,vp}} = \frac{\chi}{d^3}\left(\frac{\sigma_{\mathrm{eq}}^{\mathrm{I}}}{\sigma_{\mathrm{c}}^{\mathrm{I}}}\right)^{m} \exp\left(-\frac{\Delta G_0(\theta_{\mathrm{mis}})}{k_{\mathrm{B}}T}\left(1-\left(\frac{K\cdot\sigma_{\mathrm{eq}}^{\mathrm{M}}}{\sigma_{\mathrm{c}}^{\mathrm{M}}(\theta_{\mathrm{mis}})}\right)^{p}\right)^{q}\right), \tag{1}$$

where, d, $\sigma_{\mathrm{eq}}^{\mathrm{I}}$, $\sigma_{\mathrm{c}}^{\mathrm{I}}$, m, k_{B}, T, $\sigma_{\mathrm{eq}}^{\mathrm{M}}$, p and q represent the grain diameter, Von Mises stress in the grain interior, the grain interior flow stress at 0 K, the flow exponent, Boltzmann constant,

the absolute temperature (K), Von Mises stress in the interface, and two coefficients that characterize the shape of the dislocation emission resistance curve, respectively. The critical emission stress at 0 K and the free enthalpy of activation are represented by σ_c^M and ΔG_0, respectively. In general, both parameters depend on the misorientation angle of the grain boundary (or more generally, the grain boundary structure). The coefficient χ is given by

$$\chi = \frac{m_{dis} v_0 \delta \sin(\theta)}{(m_{dis} + m_{GB}) \iota} \tag{2}$$

where, m_{dis}, m_{GB}, v_0, δ, θ and t represent the average dislocation rest mass, the interface mass affected by a dislocation absorption event, the ledge density per unit area, the dislocation emission angle and a numerical constant, respectively. Estimates for most of the parameters introduced in Eqs. (1) and (2) can be obtained from simple reasoning based on existing theories (Capolungo et al., 2007).

Eq. (1) takes the form of a typical expression for a thermally activated mechanism, with the pre-exponential term defining the activation rate, representing the product of the frequency of the emission event by the average strain rate engendered by an absorption event. An event is considered successful if a dislocation nucleated at the grain boundary source is not reabsorbed at the emission site. Hence, in this model, every successful emission event leads to the absorption of the emitted dislocation by the grain boundary opposite to the source. The emission frequency is proportional to the number of principal interface dislocation sources which are here considered to be ledges and assumed proportional to the inverse of the square of the grain size. The average strain rate accounts for the mass transfer within the interface engendered by a single absorption event considered here as a soft collision. The exponential term describes the probability of success of a single emission event when a Boltzmann distribution is assumed.

Finally, the parameter K in Eq. (1) is included to account for the stress concentrations localized in the matrix phase. Since the Eshelbian micromechanical scheme used to perform the scale transition from the mesoscopic scale to the macroscopic scale cannot account for stress concentrations, the introduction of a stress concentration factor will lead to more realistic predictions. The impact of this modification will be evaluated in Section 4. Future studies estimating the stress concentrations at grain boundaries and triple junctions could clearly enhance the current understanding of the dislocation nucleation phenomenon.

The behavior of the matrix phase is taken as isotropic. Hence the equivalent viscoplastic strain rate, defined in Eq. (1), is related to the averaged viscoplastic strain via Prandtl–Reuss law, i.e.,

$$\dot{\varepsilon}^{M,vp} = \frac{3}{2}\left(\frac{\dot{\varepsilon}_{eq}^{M,vp}}{\sigma_{eq}^{M}}\right)\sigma_{dev}^{M} \tag{3}$$

where, σ_{dev}^{M} and $\dot{\varepsilon}^{M,vp}$ represent the deviatoric part of the average stress tensor in the matrix phase and the average viscoplastic strain rate tensor in the matrix phase, respectively. As will be shown in Section 3, estimates for the free enthalpy of activation and the critical emission stress in Eq. (1) can be retrieved via MD simulations. Let us recall that the critical emission stress is defined as the minimum stress required so that the probability of success of the dislocation emission event is equal to unity at 0 K. The free enthalpy of activation

represents the energy that must be brought into the system without the assistance of thermal activation for the emission event to be successful.

3. Molecular dynamics simulations

Two sets of MD simulations are performed to estimate the critical dislocation emission stress and the free enthalpy of activation at 0 K: (i) uniaxial tensile deformation of a planar $\Sigma 5$ $\{2\,1\,0\}$ 53.1° boundary and (ii) uniaxial tensile deformation of an interface with the same misorientation containing a ledge. The goal is to analyze the nucleation of the *first* dislocation that is emitted from the boundary. The $\Sigma 5$ $\{2\,1\,0\}$ interface is chosen because (i) the inelastic deformation of this boundary has not been studied in detail and (ii) literature is available to validate the structure of the bicrystal interface (cf. Bachurin et al., 2003). These preliminary calculations are performed to illustrate the connection between atomistic simulations and the continuum model; future MD work will evaluate a range of boundary misorientations and ledge configurations.

Naturally, dislocation emission is a thermally activated process. In general, at a given stress, the probability that a dislocation is emitted from the boundary is greater at higher temperatures due to the thermal component of the emission mechanism. However, the aim of the simulations in this work is to estimate the nucleation stress and the free enthalpy of activation for use in the model for NC deformation, both of which are defined in the model at 0 K. Thus, simulations in this work are performed at 10 K as a compromise between the ability of MD to capture a single dislocation as it is nucleated and the proposed NC model parameters. The difficulty resides in the fact that a single dislocation emission event must be captured. Hence, it is very challenging to use molecular statics to estimate both the free enthalpy of activation and the critical emission stress since simultaneous emission of multiple dislocations is possible. Also, owing to the thermally activated nature of the dislocation emission mechanism, an increase in the temperature used in the simulations leads to a decrease in the estimates of the parameters driving the mechanism. Hence, the temperature used in the simulations must be sufficiently low to attain good accuracy in the computed parameters yet greater than zero to enable the observation of single dislocation events.However, as a consequence the estimated critical nucleation stress and the free enthalpy of activation will be slightly underestimated.

Molecular mechanics (MM) simulations performed at 0 K, using the nudged elastic band method for example, may potentially lead to a more precise estimate of the energy barrier for dislocation nucleation. This approach may be pursued in future work to further validate the MD calculations presented here once a clear understanding of the interface structure after extended dislocation nucleation is established.

3.1. Interface model preparation

Fig. 2 provides a schematic illustration of the 'planar' and 'stepped' interface models considered in this work. The $\Sigma 5$ $\{2\,1\,0\}$ 53.1° boundary is created by a symmetric tilt rotation, Φ, of opposing lattice regions around the [0 0 1] crystallographic axis (the interface misorientation is measured using the [1 0 0] crystallographic direction as the reference). This particular misorientation is considered 'favored' in the structural unit model representation of interfaces (Sutton and Vitek, 1983). Two pure ledges are created along the interface plane in the stepped interface model (Fig. 1(b)). The ledge height, l_H, is

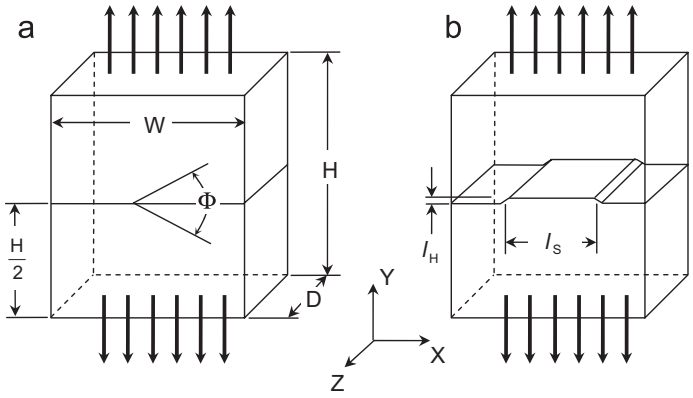

Fig. 2. Bicrystal interface models used in the present set of calculations. The interface misorientation axis is taken as the [0 0 1] crystallographic direction axis for both (a) planar and (b) stepped models. Details regarding interface model dimensions, ledge height and spacing can be found in Table 1.

Table 1
Interface model dimensions considered in the current work

Interface Type	Width, W (nm)	Height, H (nm)	Depth, D (nm)	Ledge height (nm)	Ledge spacing (nm)	Number of atoms
Planar (Σ5)	19.4	22.6	16.2	n/a	n/a	533,760
Stepped (Σ5)	19.4	22.6	16.2	0.79	9.7	533,760
Stepped 2X (Σ5)	38.8	22.6	16.2	0.79	19.4	1,067,520

taken as two times the repeating length of the superlattice of coincident sites for this misorientation (Randle, 1993). Of course, other ledge structures are possible for this misorientation, including disconnections, which are formed by appropriate combinations of step and Burgers vectors (Kurtz et al., 1999; Hirth et al., 2006). The dimensions of the interface models are prescribed as necessary to enforce periodic boundary conditions in all directions (X, Y and Z) and are presented in Table 1. Scale considerations will be discussed in Section 3.5.

Bicrystal interface models are prepared using a combination of molecular statics (mechanics) and MD simulations. Molecular statics calculations are used to refine the initial interface structures. Energy minimization is achieved using a nonlinear conjugate gradient algorithm. Obviously, it is critical that the initial interface and ledge structures are described appropriately to be able to draw definitive conclusions regarding the role of individual interface features on the dislocation nucleation process. Upon completion of the energy minimization procedure, the interface model is equilibrated using MD in the isobaric–isothermal ensemble at a pressure of 0 bar and a temperature of 10 K. In this work, the Melchionna et al. (1993) equations of motion for the NPT ensemble govern the dynamics of the system. MD simulations are then used to deform each interface model in uniaxial tension, which is applied in the Y-direction normal to the interface plane (recall

Fig. 1). The motions of the boundaries are calculated from the current and prescribed system stresses (Melchionna et al., 1993). For all simulations in this work, the boundaries perpendicular to the interface plane are specified as stress-free. Throughout the deformation process, the temperature is maintained at approximately 10 K.

Of critical importance to these calculations is the choice of the interatomic potential. We use the copper embedded-atom method (EAM) potential of Mishin et al. (2001). Two critical properties that must be well characterized by the interatomic potential to model dislocation nucleation and defect structures are the intrinsic and unstable stacking fault energies. For example, Rittner and Seidman (1996) showed that predicted interface structure can vary depending on the magnitude of the intrinsic stacking fault energy. Mishin et al. report an intrinsic stacking fault energy of 44.4 mJ/m^2 and an unstable stacking fault energy of 158 mJ/m^2, both of which compare favorably with experimental evidence and quantum calculations presented in their work.

3.2. Interface and ledge structures

Figs. 3(a) and (b) show detailed views of the planar and stepped $\Sigma5$ $\{2\,1\,0\}$ interface structures. The viewing direction is along the [0 0 1] crystallographic axis (Z-direction) and atom positions are projected into the X–Y plane for clarity. Snapshots of the atomic configurations at the interface are taken after the isobaric-isothermal equilibration procedure at 0 bar and 10 K. The structure of each interface can be readily identified by shading atoms according to their respective $\{0\,0\,1\}$ atomic plane, as indicated in the legend of Fig. 3.

The planar 53.1° interface in Fig. 3(a) is composed entirely of B′ structural units, in agreement with previous atomistic simulations that employ embedded-atom method

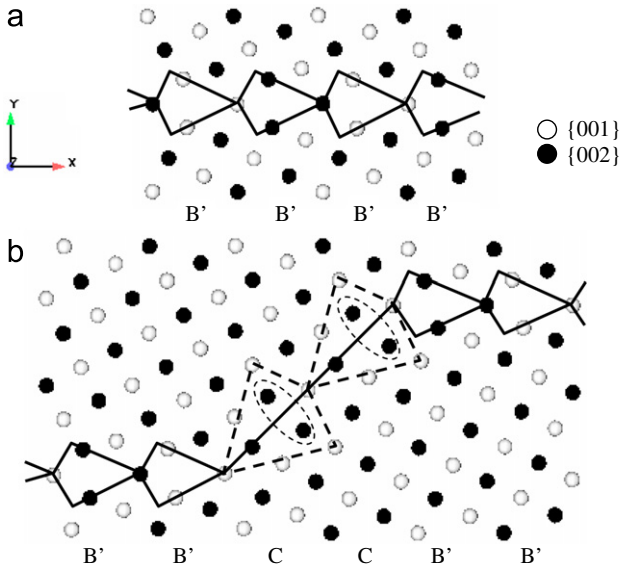

Fig. 3. Bicrystal interface structure for (a) the planar $\Sigma5$ (2 1 0) 53.1° misorientation and (b) the stepped interface with a pure ledge. The structural units for each interface are outlined along the interface plane.

interatomic potentials (Bachurin et al., 2003). It is noted that two configurations are commonly observed for this structural unit, the other being termed the B structural unit (Sutton and Vitek, 1983). The B structural unit is identical to that shown in Fig. 3(a); however, an additional atom is located in the center of the 'arrowhead' shaped feature. Supplementary energy minimization calculations are performed (although not explicitly shown in this work) to verify that the copper $\Sigma 5$ {{2 1 0} boundary composed entirely of B' structural units is accurate. Energy minimization calculations report an interfacial energy of 950 mJ/m^2 for the boundary composed entirely of B' structural units, which is lower than all other potential configurations for this particular misorientation.

A detailed image of the pure ledge structure is shown in Fig. 3(b). The pure ledge exists at a 45° angle relative to the positive X-direction, which is expected due to the symmetric nature of the lattice misorientation between crystalline regions. The height of the ledge after isobaric–isothermal equilibration is approximately 7.9 Å. Analysis of the pure ledge structure in Fig. 3(b) reveals that structural units may be defined along the step. These features are reminiscent of the C structural unit, which is associated with the $\Sigma 5$ {3 1 0} 36.9° interface (Sutton and Vitek, 1983). Additional energy minimization calculations are performed to verify that the atomic structure of the pure ledge in Fig. 3(b) is accurate. For example, the atomic density along the step may be altered by removing one atom from each pair of atoms circled in Fig. 3(b). Energy minimization calculations report an interfacial energy of 989 mJ/m^2 for a boundary with two ledges identical to that shown in Fig. 3(b) and 10253,1025 mJ/m^2 for a stepped boundary after the removal of the indicated ledge atoms. Clearly, the interface configuration shown in Fig. 3(b) is most appropriate.

3.3. Dislocation nucleation

MD simulations are used to (i) observe dislocation nucleation from the planar and stepped bicrystal interfaces, (ii) compute the stress required for dislocation nucleation, and (iii) estimate the change in interfacial energy associated with the nucleation of the first partial dislocation during the tensile deformation process. The aim is to have MD simulations provide an appropriate set of values for use in the proposed model for NC deformation, as discussed in detail in Section 2. Dislocation nucleation from ledges or steps along the interface plane is considered as a primary source for the initiation of plastic deformation in the model.

To compute the stress required for dislocation nucleation, both the planar and stepped interface models are subjected to a sequence of increasing applied uniaxial tensions perpendicular to the interface plane. Motivated by previous MD simulations of bicrystal failure (Spearot et al., 2005, 2007), the minimum applied tensile stress was taken as 5 GPa. Simulations were run for 100,000 time steps (which is equivalent to 100 ps using a timestep of 1 fs). If partial dislocation nucleation is not observed during the simulation time, the applied stress is increased by 0.1 or 0.2 GPa and the simulation is repeated until partial dislocation nucleation occurs. A similar procedure has been used in the literature to determine the stress required for dislocation nucleation in NC samples (cf. Yamakov et al., 2001). We find that the minimum uniaxial tensile stress required for partial dislocation nucleation at 10 K from the planar interface is 6.1 GPa, while the minimum uniaxial tensile stress required for partial dislocation nucleation from the stepped interface at 10 K is 5.8 GPa.

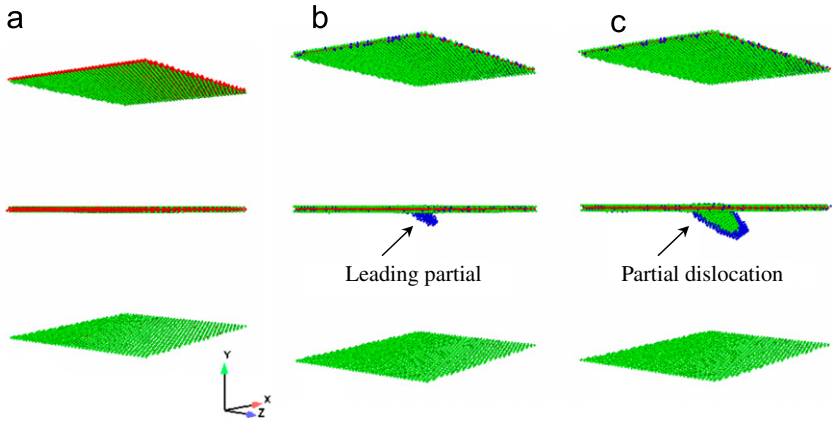

Fig. 4. (a)–(c) Nucleation of a partial dislocation loop on the primary slip system during uniaxial tension of the planar Σ5 (2 1 0) 53.1° interface model at 10 K. Atoms are colored by the centrosymmetry parameter. The interface structural units are directly involved in the dislocation nucleation process.

Snapshots of partial dislocation nucleation from the 53.1° {2 1 0} *planar* interface in copper at an applied stress of 6.1 GPa are shown in Fig. 4. Images in Figs. 4(a)–(c) are colored according to the centrosymmetry parameter (Kelchner et al., 1998); atoms with a centrosymmetry parameter close to zero are removed to facilitate viewing of the defect structures. Clearly, MD simulations are capable of capturing the first partial dislocation as it is nucleated from the interface. This partial dislocation is nucleated on one of the primary $\{1\,1\,1\}/\langle 1\,1\,2\rangle$; slip systems, in agreement with that predicted using a Schmid Factor analysis of the lattice orientation (cf. Hosford, 1993). The interior of the nucleated partial dislocation (which is shown in blue) has both edge and screw character, while the leading partial dislocation is connected back to the interface by an intrinsic stacking fault (shown in green). Nucleation of the trailing partial dislocation from the interface is not observed during the simulation time. This is characteristic of MD simulations of dislocation nucleation in copper and has been discussed at length by Van Swygenhoven and colleagues (Derlet and Van Swygenhoven, 2002; Froseth et al., 2004). To determine the magnitude of the resolved shear stress that acts on the slip plane in the direction of the partial dislocation nucleation, the unixial state of stress is resolved onto the activated $\{1\,1\,1\}$ plane in the $\langle 1\,1\,2\rangle$ slip direction. This stress is calculated as 2.58 GPa.

Note that if additional tensile deformation is applied to the interface model, dislocation nucleation will occur at other sites along the interface plane. In addition, the nucleated dislocation shown in Fig. 3(c) will propagate through the periodic boundary. We emphasize that our analysis focuses only on nucleation of the first partial dislocation.

Images of partial dislocation nucleation from the *stepped* interface with 53.1° misorientation are shown in Fig. 5. MD simulations reveal that dislocation nucleation originates from the interface ledge and occurs on one of the primary $\{1\,1\,1\}\ \langle 1\,1\,2\rangle$ slip systems. The leading partial dislocation, which has both edge and screw components, is connected back to the interface via an intrinsic stacking fault. Even though the dislocation is nucleated at the interface step, the dislocation moves along the activated slip plane, eventually incorporating regions of the interface away from the ledge (as shown in Fig. 5(c)). Again, nucleation of the trailing partial dislocation from the interface is not

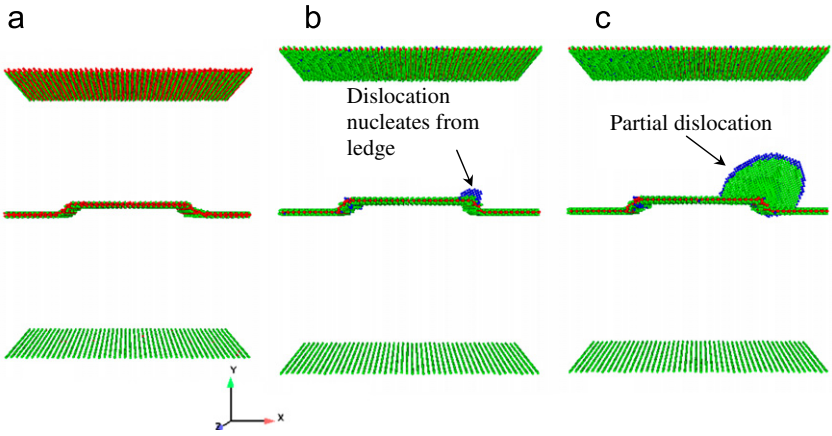

Fig. 5. (a)–(c) Nucleation of a partial dislocation loop during uniaxial tension of the stepped interface model at 10 K. Atoms are colored by the centrosymmetry parameter. The partial dislocation loop originates from the interface ledge on the primary slip system for this misorientation.

observed during the simulation time. To determine the magnitude of the stress that acts on the slip plane in the direction of the partial dislocation nucleation, the uniaxial state of stress is resolved onto the activated $\{1\,1\,1\}$ plane in the $\langle 1\,1\,2\rangle$ slip direction. The stress required for partial dislocation nucleation is calculated as 2.45 GPa.

3.4. Dislocation nucleation energy

The third objective of the MD simulations presented in this work is to compute the change in interfacial energy associated with nucleation of the first partial dislocation from the planar and stepped interfaces. At 10 K, the magnitude of the change in interfacial energy is approximately equal to the free enthalpy of activation, which is required in the continuum model. Unfortunately, it is not possible to compute this quantity directly from the total energy of the MD simulation because both interface and lattice stretch contribute to the change in total energy during the tensile deformation process. Instead, interface energy is computed by considering the energy at the boundary between the two crystalline regions that is in excess of the intrinsic energy of the bulk lattices (Muller and Saul, 2004; Nozieres and Wolf, 1988; Wolf and Nozieres, 1988). This concept is schematically illustrated in Fig. 6(a) and is mathematically expressed as

$$E^{\text{int}} = \int_{y_A}^{y_B} e(y)\mathrm{d}y - e_A(Y_0 - y_A) - e_B(y_B - Y) \tag{4}$$

In Eq. (4), $e(y)$ is the energy profile normal to the interface, e_A is the bulk energy in region A and e_B is the bulk energy in region B. In this work, regions A and B represent the atoms that comprise the lower and upper crystalline regions, respectively. The $\{2\,1\,0\}$ interface plane may include atoms from either region (interface configuration is determined via the energy minimization procedure), i.e., all atoms in the MD simulations are considered in the calculation of excess interface energy. The vertical locations Y_0, y_A and

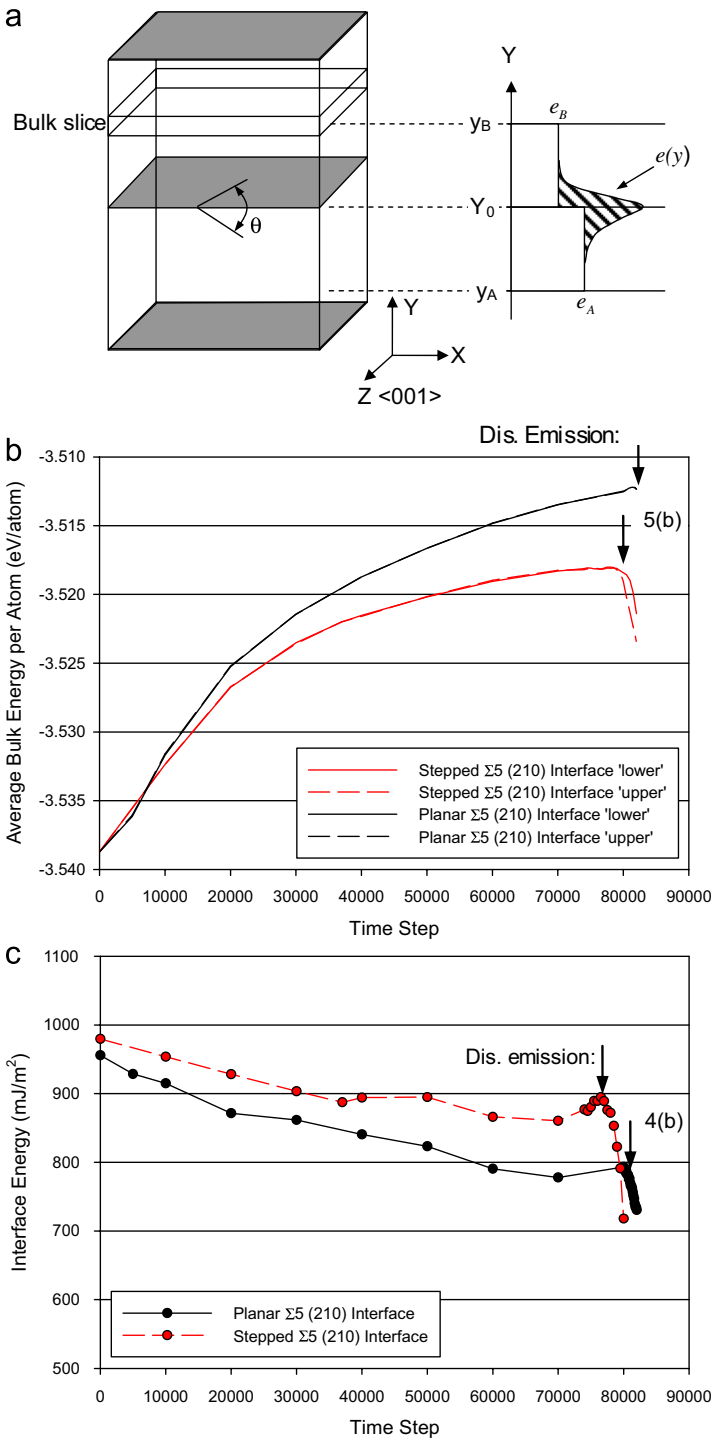

Fig. 6. (a) Schematic illustration of the calculation of interface 'excess' energy; (b) average energy per atom within the bulk (away from the interface) for the planar Σ5 (2 1 0) interface at an applied tensile stress of 6.1 GPa and the stepped interface at an applied tensile stress of 5.8 GPa; (c) evolution of the interface energy as a function of MD time step showing that the interface excess energy decreases during the tensile deformation process.

y_B are defined schematically in Fig. 6(a). Essentially, the bulk energy of the opposing lattice regions is subtracted from the total energy distribution. The remaining excess quantity is defined as the interface energy (Muller and Saul, 2004; Nozieres and Wolf, 1988; Wolf and Nozieres, 1988). Note that this definition does not require the introduction of an interface volume or region around the bicrystal boundary as long as y_A and y_B are larger than the region which is distorted by the presence of the planar defect. In addition, this approach is applicable for asymmetric boundaries because the bulk energies of the opposing lattice regions are computed and handled separately.

Slight modifications are required in order to apply Eq. (4) to discrete atomistic systems. Notably, the integral of the energy profile must be replaced by a summation over a set of atoms within each crystalline region, i.e.,

$$E^{\text{int}} = \sum_{i=1}^{N_A} [e_i - e_A] + \sum_{i=1}^{N_B} [e_i - e_B] \tag{5}$$

where, N_A and N_B are the number of atoms in regions A and B, respectively. The bulk energies, e_A and e_B, are determined by averaging the individual atomic energies of a 'slice' of atoms positioned sufficiently far away from the interface such that the presence of the boundary is not detected (beyond y_A or y_B in Fig. 6(a)). The calculation of bulk energies is performed at every output time step during the MD simulation, as shown in Fig. 6(b) for both the planar and stepped $\Sigma 5$ (2 1 0) boundaries. Fig. 6(b) shows that the energy of the bulk region increases during tensile deformation and then decreases once a dislocation is nucleated from the boundary. The simulation is halted shortly after the first dislocation is nucleated. As expected (due to the symmetric tilt rotation of the boundary), the behavior of the bulk lattice in both 'upper' and 'lower' crystalline regions is nearly identical prior to dislocation nucleation. This provides definitive evidence that the averaging region used to determine the bulk energy evolution is sufficiently far away from the boundary.

Using the calculated bulk energies, an excess energy is computed for each atom within the interface model. The sum of these excess quantities is defined as the interface energy (Eq. (5)). The evolution of the interface energy during the deformation process is shown in Fig. 6(c). Initial values for the interface energy are in agreement with energy minimization calculations for both planar and stepped interfaces, indicating that the isobaric–isothermal equilibration procedure did not disturb the computed interface structure. In general, the interface excess energy decreases as a function of the MD time step. Just prior to dislocation nucleation, there appears to be a slight increase in the excess interface energy, following by a sharp decrease after the dislocation nucleation event. Recall that a decrease in the excess interface energy does not imply that the total energy of the interface decreases. In fact, the total energy of the interface region does increase during the deformation process; however, the energy of the bulk lattice regions increases more significantly than that of the interface. The observation of a negative change in the excess interface energy as a function of applied stress is in agreement with the discussion provided in Muller and Saul (2004). A negative change in the excess quantity corresponds to elastic relaxation from an unstable to a stable state. This is the case when interface forces (or stresses) are applied to a solid/solid interface and the final configuration is considered the relaxed (equilibrium) state. In other words, the initial configuration is considered 'unstable' with respect to the applied stress (Muller and Saul, 2004). It is important to emphasize that this does not indicate that the initial configuration is unstable with respect to dislocation

nucleation. Physically, the change in excess energy measured via molecular simulations shall be considered as the required energy change to compensate the energy barrier to the dislocation emission process. Hence, the negative of change in the excess energy is chosen here to approximate the free enthalpy of activation. It is noted that a rigorous calculation of the free enthalpy of activation entails the quantification of the change in energy of the sole dislocation. However, the grain boundary structure sustains local rearrangements during the nucleation event which adds considerable complexity to the energy landscape in quantification of the free enthalpy of activation. Future calculations will be aimed at studying the pre-dislocation nucleation evolution of the interface structure to observe how the interface evolves to a position apt for dislocation nucleation at a given applied stress.

The magnitude of the change in interfacial energy during the dislocation emission process is simply defined as the initial energy of the interface (unstressed state at isobaric–isothermal equilibrium) minus the interface energy at the point of dislocation nucleation. According to Fig. 6(c), the magnitude of the change in interfacial energy associated with dislocation emission from the planar $\Sigma5$ (2 1 0) boundary is approximately $173.2\,\mathrm{mJ/m^2}$ while the magnitude of the change in interfacial energy associated with dislocation nucleation from the stepped $\Sigma5$ (2 1 0) boundary is approximately $103.8\,\mathrm{mJ/m^2}$. Thus, MD simulations appear capable of capturing the critical aspects of the dislocation nucleation process as they indicate that slightly lower levels of applied stress are necessary to nucleate a dislocation from an interface with a pure ledge as compared with a perfectly planar interface. Furthermore, the energy barrier for dislocation nucleation is lower for the interface with a pure ledge as compared with the planar bicrystal interface, emphasizing the role of interface ledges in the dislocation nucleation process. Section 4 will further elaborate on how these quantities are used in the model for NC deformation.

3.5. MD simulation scale considerations

The chosen dimensions of the interface structure and the simulation cell may potentially have an effect on the MD results. Four critical dimensions must be evaluated: the spacing between interface ledges, the simulation cell width, height and depth. Based on previous MD simulations (Spearot et al., 2005, 2007), the dimensions of the *planar* interface model should be adequate to study the nucleation of the first partial dislocation from the interface. In the Z-direction, the depth of the interface model includes 80 (0 0 1) atomic planes, which is sufficient to have little effect on the 3D nature of dislocation nucleation. In the X-direction, the planar interface includes many interface periods. Increasing the dimensions of the planar interface model in either of these directions will not affect the simulation results (cf. Spearot et al., (2007)). The use of periodic boundary conditions in the Y-direction introduces a second interface into the model, which in turn gives rise to forces on interfacial dislocations. The stress field for a symmetric tilt boundary, such as that studied in this work, decreases exponentially away from the interface (Hirth and Lothe, 1982). The spacing between interfaces, $H/2$, is sufficiently large so that the effect on nucleation of the *first* partial dislocation will be minimal.

On the other hand, particular care must be exercised when simulating dislocation nucleation from the *stepped* interface. The use of periodic boundary conditions in the X-direction replicates an infinite array of steps along the interface plane, each of which has a long range stress field (Hirth and Lothe, 1982). The spacing between interface steps must be sufficiently large such that the stress required for dislocation nucleation and the change

in interfacial energy associated with dislocation nucleation are not dramatically affected. To validate the dimensions of the stepped interface model, additional simulations are performed using a simulation cell with dimensions that are doubled in the X-direction (both the total width and the spacing between interfaces ledges). The exact dimensions of this model are provided in Table 1. MD simulations indicate that dislocation nucleation occurs at an applied uniaxial tensile stress of 5.8 GPa, identical to that found using the smaller interface model, with dislocation nucleation originating at the ledge and occurring on the primary slip systems. The change in interfacial energy associated with dislocation nucleation from the stepped $\Sigma 5$ (2 1 0) boundary (using the same procedure as detailed in Section 3.4) is approximately 103.2 mJ/m^2, which is extremely close to the value computed using the smaller stepped interface model.

4. Model for NC deformation

As illustrated in Fig. 1, in this work a NC material is represented as a two-phase composite model where the inclusion phase represents grain interiors and the matrix phase represents both grain boundaries and triple junctions (Capolungo et al., 2006). Hence, in this approach the effects of texture, grain orientation, grain size distribution and grain boundary misorientations distribution are neglected. However, the present model could be extended to account for the previously mentioned microstructural parameters with the introduction of distribution functions for all parameters. This would transform the two-phase composite approach into an n-phase approach.

4.1. Inclusion behavior

Inclusions deform elasto-viscoplastically via dislocation glide mechanisms for which the typical expressions describing the hardening behavior are modified to take into account the long range effect of grain boundaries on the flow stress at 0 K. Hence, the equivalent viscoplastic strain rate in the inclusion phase, $\dot{\varepsilon}_{eq}^{I,VP}$, is given by the typical power law hardening equation

$$\dot{\varepsilon}_{eq}^{I,VP} = \dot{\varepsilon}_0 \left(\frac{\sigma_{eq}^{I}}{\sigma_f} \right)^m, \tag{6}$$

where $\sigma_{eq}^{I}, \dot{\varepsilon}_0, m, \sigma_f$ denote the equivalent stress in the inclusion phase, a reference strain rate (constant), the flow exponent, and the flow stress at 0 K, respectively. The flow exponent has a weak dependence on the dislocation density; hence, in this study m is taken as a constant. The flow stress at zero Kelvin accounts for both the effect of stored dislocations and the stresses engendered by grain boundaries, i.e.,

$$\sigma_f = \alpha M G b \sqrt{\rho} + \beta / \sqrt{d}, \tag{7}$$

where α s a constant, and G, M, ρ, b, β and d respectively denote the shear modulus, the Taylor factor, the dislocation density, the magnitude of the Burgers vector, the Hall-Petch slope, and the grain size. The evolution of the dislocation density with the local equivalent viscoplastic strain rate accounts for the simultaneous effect of athermal storage and thermally activated dislocation annihilation. Athermal storage results from the decrease in the mean free path of mobile dislocations engendered by the presence of grain boundaries

and stored dislocations, which are described by the first and second terms on the right hand side in the following equation:

$$\frac{\mathrm{d}\rho}{\mathrm{d}\varepsilon_{\mathrm{eq}}^{\mathrm{I,vp}}} = M\left(\frac{k_0}{d} + k_1\sqrt{\rho} - k_{20}\left(\frac{\dot{\varepsilon}_{\mathrm{eq}}^{\mathrm{I,vp}}}{\dot{\varepsilon}_*}\right)^{-1/n}\rho\right). \tag{8}$$

In Eq. (8), k_0, k_1 and k_{20} are constants. The exponent, n, is constant at a given temperature and $\dot{\varepsilon}_*$ is a normalization strain rate. Isotropic hardening is also assumed and the equivalent viscoplastic strain rate is related to the viscoplastic strain rate tensor

$$\dot{\varepsilon}^{\mathrm{I,vp}} = \frac{3}{2}\left(\frac{\dot{\varepsilon}_{\mathrm{eq}}^{\mathrm{I,vp}}}{\sigma_{\mathrm{eq}}^{\mathrm{I}}}\right)\sigma_{\mathrm{dev}}^{\mathrm{I}}, \tag{9}$$

where, $\sigma_{\mathrm{dev}}^{\mathrm{I}}$ and $\dot{\varepsilon}^{\mathrm{I,vp}}$ represent the deviatoric part of the average stress tensor in the inclusion phase and the average viscoplastic strain rate tensor in the inclusion phase, respectively.

Let us note that dislocation activity, via storage and annihilation, is known to decrease in NC materials. As mentioned in the introduction, it was shown experimentally that NC materials with grain size in the range of ~30 nm are virtually dislocation free (Kumar et al., 2003), at least within grain interiors. Hence, the above description of the response of the inclusion phase will lead to an overestimation of the state of stress in the inclusion phase. However, the micromechanical scheme, to be presented in the following section, decreases the contribution of grain interiors to the benefit of that of the matrix phase when the grain size is reduced.

4.2. Scale transition from the mesoscopic scale to the macroscopic scale

The parameters extracted from MD simulations are utilized in a recently developed model for NC deformation (Capolungo et al., 2006), enabling the scale transition via the use of a secant self-consistent scheme (Berbenni et al., 2004). The problem of interaction between inclusion and matrix phases is solved by taking into account the space–time coupling of the constitutive laws via the introduction of a translated viscoplastic strain rate. Inclusions are taken as spherical and the volume fraction of inclusions is given by

$$f = \left(\frac{d}{d+w}\right)^3, \tag{10}$$

where d and w represent the grain size and grain boundary thickness, respectively. In what follows, the superscript r denotes either the inclusion phase, noted I, or the matrix phase, noted M. The local behaviors of the inclusion and matrix phase are elastic–viscoplastic and written as

$$\dot{\varepsilon}^{\mathrm{r}} = \dot{\varepsilon}^{\mathrm{e,r}} + \dot{\varepsilon}^{\mathrm{vp,r}} = s^{\mathrm{r}} : \dot{\sigma}^{\mathrm{r}} + m^{\mathrm{r}} : \sigma^{\mathrm{r}}, \tag{11}$$

In Eq. (11), $\dot{\varepsilon}^{\mathrm{e,r}}$ and $\dot{\varepsilon}^{\mathrm{vp,r}}$ denote the average elastic and viscoplastic strain rate tensors, respectively. The parameters S^{r} and m^{r} denote the local elastic compliance tensor and the fourth order viscosity tensor, while $\sigma^{\mathrm{r}}$and $\dot{\sigma}^{\mathrm{r}}$ denote the average local stress tensor and its rate, respectively. The behavior of both phases is assumed incompressible. Considering isotropic hardening, the viscosity tensor is expressed by

$$\boldsymbol{m}^{\mathrm{r}} = \frac{1}{2\eta^{\mathrm{r}}}\boldsymbol{K}, \tag{12}$$

where $\boldsymbol{K}$ is a fourth order tensor defined as: $K_{ijkl} = \frac{1}{2}(\delta_{ik}\delta_{jl} + \delta_{il}\delta_{jk}) - \frac{1}{3}\delta_{ij}\delta_{kl}$ and δ is the Kronecker symbol. The viscosity coefficient is given by

$$\eta^{\mathrm{r}} = \frac{\sigma^{\mathrm{r}}_{\mathrm{eq}}}{3\dot{\varepsilon}^{\mathrm{r,vp}}_{\mathrm{eq}}} \tag{13}$$

Similarly, the macroscopic behavior is elastic–viscoplastic and written as

$$\dot{\boldsymbol{E}} = \dot{\boldsymbol{E}}^{\mathrm{e}} + \dot{\boldsymbol{E}}^{\mathrm{vp}} = \boldsymbol{S}^{\mathrm{e}} : \dot{\Sigma} + \boldsymbol{M}^{\mathrm{e}} : \Sigma, \tag{14}$$

where $\dot{\boldsymbol{E}}$, $\dot{\boldsymbol{E}}^{\mathrm{e}}$, $\dot{\boldsymbol{E}}^{\mathrm{vp}}$, $\dot{\boldsymbol{S}}^{\mathrm{e}}$, $\boldsymbol{M}^{\mathrm{e}}$, Σ and $\dot{\Sigma}$ denote the second order macroscopic strain rate tensor, the second order macroscopic elastic strain rate tensor, the second order macroscopic viscoplastic strain rate tensor, the fourth order effective compliance tensor, the fourth order viscosity tensor, the second order macroscopic stress tensor and its rate, respectively. The average local behavior of the different phases is related to the global behavior of the material through the concentration relation,

$$\begin{aligned}\dot{e}^{\mathrm{r}} = {} & \boldsymbol{A}^{\mathrm{Cer}} : (\dot{\boldsymbol{E}} - \dot{\boldsymbol{E}}^{\mathrm{vp}}) + \boldsymbol{A}^{\mathrm{Cer}} : \boldsymbol{A}^{\mathrm{Ber}} : \dot{\boldsymbol{E}}^{\mathrm{vp}} \\ & + \boldsymbol{A}^{\mathrm{Cer}} : \boldsymbol{S}^{\mathrm{E}} : \boldsymbol{S}^{\mathrm{e}} : (\boldsymbol{C}^{\mathrm{r}} : \dot{e}^{\mathrm{vp,r}} - \boldsymbol{C}^{\mathrm{e}} : \boldsymbol{A}^{\mathrm{Ber}} : \dot{\boldsymbol{E}}^{\mathrm{vp}}).\end{aligned} \tag{15}$$

In Eq. (15), $\boldsymbol{S}^{\mathrm{E}}$, $\boldsymbol{A}^{\mathrm{Cer}}$, A^{Ber}, $\boldsymbol{S}^{\mathrm{e}}$ and its inverse $\boldsymbol{C}^{\mathrm{e}}$ denote Eshelby's tensor, the fourth order elastic concentration tensor, the fourth order viscoplastic concentration tensor, the macroscopic compliance tensor and its inverse, respectively. From Hooke's Law, one obtains (after some algebra)

$$\dot{\boldsymbol{\sigma}} = \boldsymbol{C}^{\mathrm{r}} : \boldsymbol{A}^{\mathrm{Cer}} : \boldsymbol{S}^{\mathrm{e}} : \dot{\Sigma} + \boldsymbol{C}^{\mathrm{r}} : \boldsymbol{A}^{\mathrm{Cer}} : (\boldsymbol{S}^{\mathrm{E}} - \boldsymbol{I}) : (\dot{\varepsilon}^{\mathrm{vp,r}} - \boldsymbol{A}^{\mathrm{Ber}} : \dot{\boldsymbol{E}}^{\mathrm{vp}}). \tag{16}$$

Here, $\boldsymbol{I}$ represents the fourth order identity tensor. The effective elasticity tensor, $\boldsymbol{C}^{e}$, is directly evaluated by using the self-consistent scheme, leading to

$$\boldsymbol{C}^{e} = \overline{\boldsymbol{C}^{r} : \boldsymbol{A}^{\mathrm{Cer}}}, \tag{17}$$

where the overbar denotes the volume-average. The elastic concentration tensors are given by

$$\boldsymbol{A}^{\mathrm{Cer}} = [\boldsymbol{I} + \boldsymbol{S}^{\mathrm{E}} : \boldsymbol{C}^{\mathrm{e}} : (\boldsymbol{C}^{\mathrm{r}} - \boldsymbol{C}^{\mathrm{e}})]^{-1}, \tag{18}$$

Using the self-consistent scheme, the effective viscosity tensor, and its inverse $\boldsymbol{B}^{e}$, can be obtained as

$$\boldsymbol{B}^{\mathrm{e}} = \overline{\boldsymbol{B}^{\mathrm{r}} : \boldsymbol{B}^{\mathrm{Cer}}}, \tag{19}$$

where $\boldsymbol{B}^{\mathrm{r}}$ denotes the inverse of the local viscosity tensor for the inclusion and matrix phase. The localization tensor of the viscoplastic deformation is defined as

$$\boldsymbol{A}^{\mathrm{Ber}} = \left[\boldsymbol{I} + \boldsymbol{S}^{\mathrm{E}} : \boldsymbol{B}^{\mathrm{e}} : (\boldsymbol{b}^{\mathrm{r}} - \boldsymbol{B}^{\mathrm{e}})\right]^{-1}. \tag{20}$$

Additional information and discussion regarding the secant self-consistent scheme can be found in references by Berbenni et al. (2004).

4.3. Results

The model is applied to the case of pure NC copper using the model parameters as given in Capolungo et al. (2006), which are summarized for convenience in Table 2.

4.3.1. Primary interface dislocation sources

The probability of successful dislocation emission can be extracted from the exponential term in Eq. (1). The parameters estimated from MD for use in this calculation are summarized in Table 3. Note that the free enthalpy of activation per unit area must be multiplied by the grain boundary area for use in the NC model. The parameters p and q are chosen to obtain a perfect plastic response of the grain boundary phase; more precise estimation of these parameters will be subject to future study.

Fig. 7 shows the probability of success of a dislocation emission event versus the average applied equivalent stress acting on the matrix phase. The solid curves correspond to a 100 nm grain size while the dashed curves correspond to a 10 nm grain size. The effect of stress heterogeneity is not considered here as K is set equal to unity.

The results in Fig. 7 clearly show that the emission event occurs only at high stress levels (>2 GPa.). Hence, in both the case of a planar interface and the case of a stepped interface, the emission event will occur for $\Sigma5$ grain boundary segments only at very small grain sizes, when the stress fields are higher due to the 'hardened' behavior of grain interiors engendered by both the reduction in the mean free path of dislocations and the effect of grain boundaries on the yield stress of the grain interiors at 0 K. The probability of successful emission increases sharply prior to the critical emission stress; however, the slopes depend on both parameters p and q, which characterize the free enthalpy of activation. In this work, the non-dimensional parameters p and q describe the 'shape' of the emission diagram and are chosen to result in a rather abrupt response, leading to $p = 1.0$ and $q = 1.5$ (Kocks et al., 1975). This plot reemphasizes that ledges are the primary dislocation sources, in the case of $\Sigma5$ $\{2\,1\,0\}$ boundaries, since at a given stress state the probability of successful emission remains higher than that in perfect planar boundaries. Note that this result may depend on the misorientation angle of the grain boundary, which can dramatically affect the interface structure. Finally, let us note that the indirect effect of grain size on the free enthalpy of activation (calculated as the product of the free enthalpy of activation per unit area multiplied by the grain boundary area) does not have a major influence on the probability of dislocation emission.

Table 2
Model parameters

Inclusion phase	$m = 230$	$n = 21.25$	$\alpha = 0.33$	$M = 3.06$
	$b = 0.257$ nm	$\beta = 0.11$ MPA m$^{-1/2}$	$k = 3.9$ E9 m^{-1}	$k_1 = 1.$E10 m^{-1}
	$k_{20} = 330.$	$\dot{\varepsilon}_* = 1/s$	$\dot{\varepsilon}_0 = 0.005\,\mathrm{s}^{-1}$	$\mu^I = 38$ GPa
Matrix Phase	$m_{\mathrm{dis}} = 3.15\,\mathrm{pN\,ps^2/\AA^2}$	$\delta = 40$	$v_0 = 0.03$	$t = 1/2$
	$m_{\mathrm{GB}} = \pi \cdot \frac{w^2}{4} \cdot \iota \cdot \rho_{\mathrm{GB}}$	$\rho_{\mathrm{GB}} = 7.61\,\mathrm{g\,cm^3}$	$\mu^{\mathrm{M}} = 30$ GPa	$W = 1$ nm

Table 3
Parameters defining the probability of dislocation emission

Perfect planar interface	$\Delta G_0 = 173.2\,\mathrm{mj/m^2}$	$\sigma_c^{\mathrm{M}} = 2580$ MPa	$p = 1$	$q = 1.5$
Stepped interface	$\Delta G_0 = 103.2\,\mathrm{mj/m^2}$	$\sigma_c^{\mathrm{M}} = 2450$ MPa	$p = 1$	$q = 1.5$

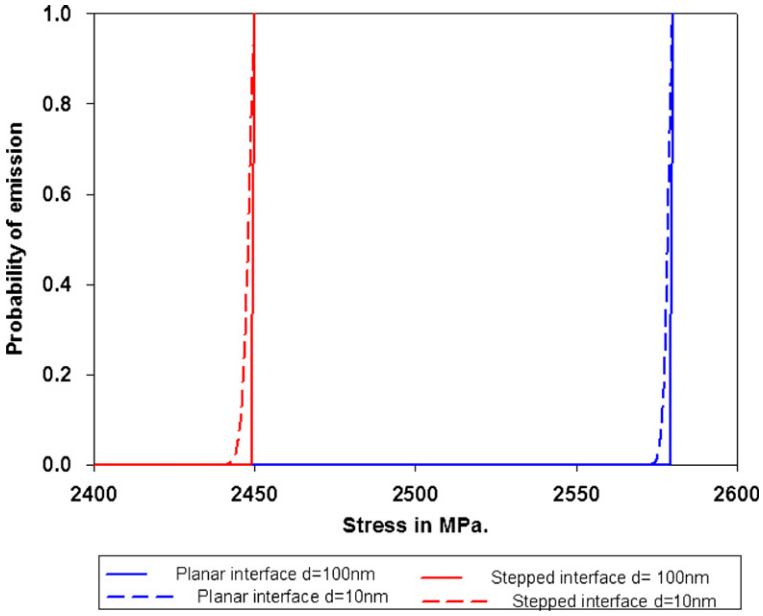

Fig. 7. Probability of successful dislocation emission versus stress for a perfect planar interface and a stepped interface at 100 and 10 nm grain sizes.

As can be observed in Fig. 7, dislocation emission is activated at extremely high stresses which cannot be predicted with traditional Eshelbian micromechanics. In general, stress concentrations at grain boundaries and triple junctions can result from the presence of additional defects in the structure (e.g. impurity atoms, nanovoids or cracks) or may result naturally from the geometry of the boundary misorientation. These effects are incorporated in the stress concentration factor K in Eq. (1). The effect of K on the probability of emission is plotted in Fig. 8. As expected, increasing the stress concentration factor will decrease the stress level required to activate the dislocation emission process.

4.3.2. Effect of grain size on yield stress

The NC model is applied to predict the evolution of the yield stress versus the inverse of the square root of the grain size. The yield strength is approximated, with the use of the offset definition, as the stress at 0.2% plastic strain. The strain rate imposed in the simulation is set to $0.001\,s^{-1}$. The results are presented in Fig. 9 where the black solid curve represents the case $K = 1$ and the black dashed curve represents the case where $K = 2$. The prediction given by the Hall–Petch relation is represented by the red dashed curve.

When stress concentrations are ignored ($K = 1$), the model is in general agreement with the Hall–Petch relation which predicts a linear increase of yield stress with an increase in inverse of the square root of the grain size. Hence, if stress concentrations are neglected in the model, the grain boundary dislocation emission mechanism cannot be activated in the quasistatic range at room temperature. Recall that in the NC model, dislocation emission results in the activation of the grain boundary dislocation absorption mechanism, which leads to mass transfer within the grain boundary. Consequently, if dislocation emission is

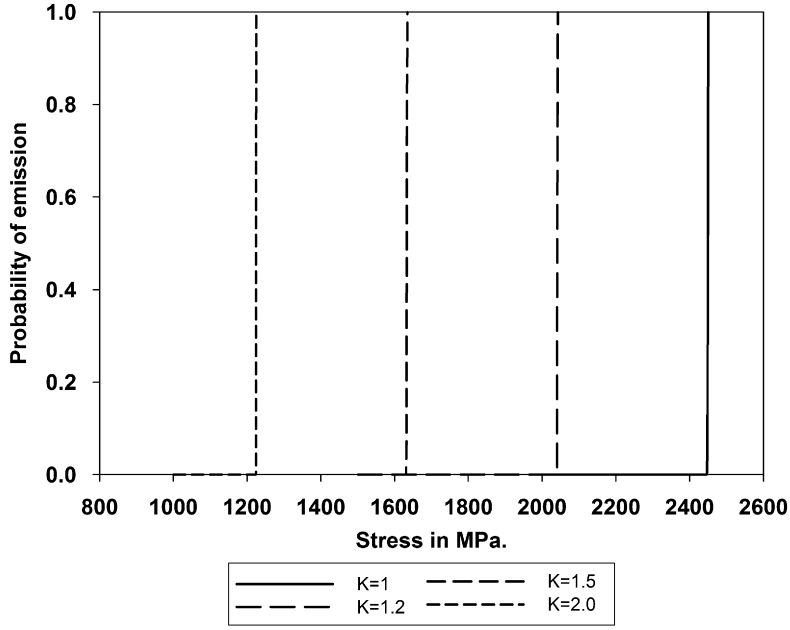

Fig. 8. Effect of stress concentrations on the probability of successful emission from a stepped interface.

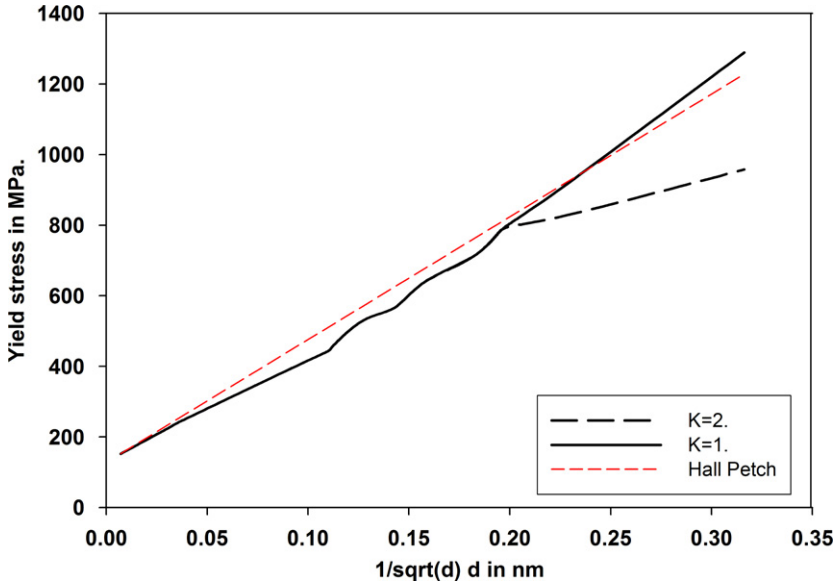

Fig. 9. Effect of stress concentration factors on the size dependent yield stress.

not activated then the breakdown in the Hall–Petch relation cannot occur. However, recall that the size effect in the initial dislocation density is not accounted for in this model. Hence, in the NC range, when the grain interiors are virtually dislocation free, the critical flow stress within the grain interiors will be considerably lower than in the present study.

Lower flow stresses in the grain interiors will inevitably lead to a softer macroscopic behavior of the NC material. Nonetheless, these results suggest that in a defect free material, where one expects low stress concentrations at the grain boundaries, grain boundary sliding could very well be the only plastic deformation mechanism available to sustain a macroscopically applied stress or strain. Moreover, the grain boundary sliding process would not be accommodated by the mass transfer engendered by dislocation absorption. MD simulations of a wider range of grain boundary structures must be performed in order to further explore the issues in the preceding discussion.

As can be observed in Fig. 9, by setting the stress concentration factor to 2, the breakdown of the Hall–Petch relation is successfully predicted and occurs at a critical grain size $d \sim 25$ nm. Fig. 10 shows the stress strain response of the inclusion phase (red curve), the matrix phase (blue curve) and the macroscopic prediction (black curve) with a 10 nm grain size and an applied 0.001 s^{-1} strain rate. Apparently, stress concentrations in the matrix phase will activate the grain boundary dislocation emission and absorption mechanisms. Hence, the behavior of the matrix phase becomes relatively softer compared to that of the inclusion phase. Since at small grain sizes the volume fraction of the matrix phase becomes non-negligible, the softer behavior of the matrix phase will lead to a softer macroscopic response leading to the predicted breakdown of the Hall–Petch relation. Experiments on 91.7% dense inert gas condensed Pd with 30 nm grain size have shown the simultaneous activity of grain boundary dislocation emission and accommodated grain boundary sliding (Markmann et al., 2003). In these samples, stress concentrations would be enhanced by voids present within the grain boundaries which would result in the activation of the dislocation emission and absorption processes. The grain boundary dislocation absorption process could serve as an accommodation mechanism to grain boundary sliding which would rationalize the observation that grain boundary decohesion was not experimentally detected in these samples.

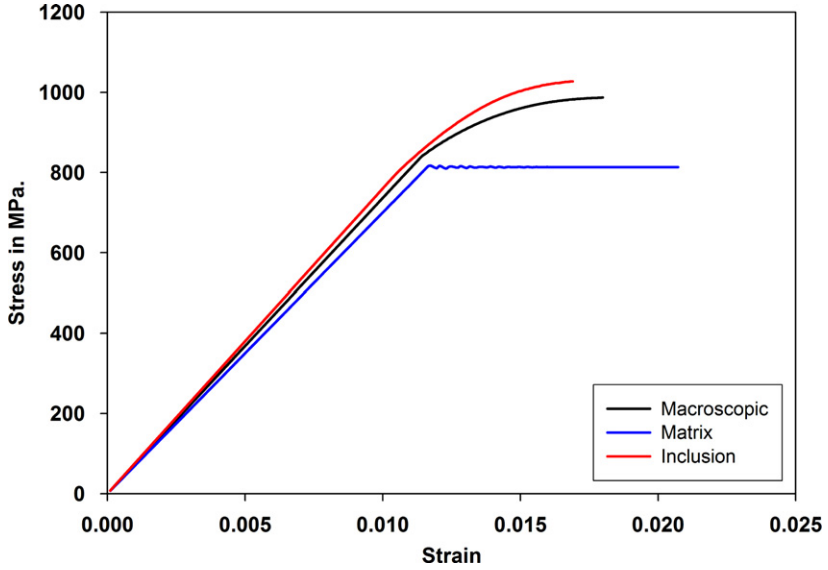

Fig. 10. Tensile predictions of a 10 nm NC copper sample with 10^{-3} s^{-1} strain rate and stress concentration factor $K = 2$.

Finally, note that the model predictions presented in Figs. 9 and 10 shall be considered as idealized cases for deformation in NC samples. Specifically, in a real NC sample, the spatial distribution of stress concentrations will obviously not be homogeneous along the grain boundaries. Hence, regions such as triple junctions are expected to exhibit higher stress concentrations and be more prone to dislocation emission than bicrystalline regions along the grain boundary.

To extend the applicability of this model, two additional phenomena must be taken into consideration: (i) a relationship between interfacial yield stress and interface structure must be developed as only one grain boundary geometry is considered in this work and (ii) the influence of other defects in the grain boundary (such as impurities and nanoscale porosity beyond that which is associated with the interface misorientation, including triple junctions), which could lower the calculated value of the critical emission stress and the free enthalpy of activation. It is possible that the high nucleation stresses computed in this work can be attributed to the fact that the simulation only considers a symmetric boundary deformed in tension. For more general high−angle boundaries (with both tilt and twist characteristics, as well as asymmetric angle of inclination) under more complex loading conditions, the interface structure may promote dislocation nucleation at much lower stresses for certain types of boundaries. Consequently, the dislocation emission mechanism would play a much more substantial role in the breakdown of the Hall–Petch relationship. Finally, the model does not yet incorporate the sliding of unaccommodated grains by vacancy diffusion, which occurs at very small grain sizes and potentially leads to material failure.

5. Conclusions

In this work, MD simulations and continuum micromechanics modeling are coupled in order to identify the primary interface dislocation sources (perfect planar interface versus stepped interface) and to quantify the macroscopic effect of dislocation emission and absorption mechanisms on NC deformation. Two types of interfaces are considered: a planar symmetric $\Sigma 5$ $\{2\,1\,0\}$ 53.1° interface and a boundary with the same interface misorientation that contains a ledge. Simulations indicate that for this particular interface geometry, grain boundary ledges are more favorable as dislocation sources than planar regions of the boundary. To facilitate a connection to the continuum model for NC deformation, two parameters are extracted from the simulation: (i) the critical stress required for dislocation emission and (ii) the change in interfacial energy associated with the nucleation of the first partial dislocation (approximation of the free enthalpy of activation). MD simulations reveal that even perfect grain boundaries can act as sources (cf. Spearot et al., 2005; Spearot et al., 2007).

The model for NC deformation accounts for the thermally activated grain boundary dislocation emission mechanism from primary dislocation sources. Assumptions are made regarding absorption. In order to account for the heterogeneity of the stress and strain states within the grain boundaries, which cannot be addressed directly with the micromechanical scheme used in this study, a stress concentration factor is introduced in the constitutive law of the matrix phase to provide more realistic estimates of the emission process. Model predictions suggest that the activation of the grain boundary dislocation emission process will depend on the details of the grain boundaries (diameter of grain interior and interface structure) in NC samples. When stress concentrations are

neglected in the micromechanical model, it is shown that for this particular interface misorientation the coupled emission and absorption event does not contribute to the breakdown of the Hall–Petch relation at small grain sizes. On the contrary, when stress concentrations are accounted for in the modified micromechanical model, grain boundary dislocation emission and absorption is activated, resulting in a softer macroscopic response of the material. The model does not account for grain boundary migration, grain growth, and coalescence.

Let us recall that this model accounts for a single symmetric CSL grain boundary and the effect of ledges on this particular grain boundary. A more realistic description of a range of likely grain boundaries is necessary to predict precisely the contribution of grain boundary dislocation emission. Nonetheless, since most grain boundaries in NC materials exhibit large misorientations angles, similarly to the grain boundary used in this study, with critical stress typically ranging between $\sim$1.9 and $\sim$3 GPa, the present model allows a qualitative prediction of the dislocation emission phenomenon.

There are several possible directions to address the issue of the high dislocation nucleation stress from MD calculations. First, it is acknowledged that such idealized MD calculations do not acknowledge the potentially potent role of impurities present in actual NC materials on reduction of the enthalpy of nucleation. Second, a much broader range of grain boundary structures should be considered beyond the $\Sigma 5$ boundary examined here, as some of them may have much lower nucleation thresholds (Sansoz and Molinari, 2005). Simulations should be extended to study a wider range of interface geometries and potential interfacial defects to generalize the model predictions. Third, the present study clearly emphasizes the need for novel extensions of self-consistent micromechanical schemes that enable the scale transition from the mesoscopic to the macroscopic scale accounting for the local inhomogeneous stress and strain states within the phases. Finally, the effects of twinning as well as dislocation emission should be considered in the micromechanical model, as this is a competing deformation mode in the NC regime for Cu. Twinning effects are captured, of course, using MD simulations.

Acknowledgments

The authors would like to thank Dr. E. Busso for helpful discussions. D.L. McDowell is grateful for the support of the Carter N. Paden, Jr. Distinguished Chair in Metals Processing.

References

Arsenlis, A., Parks, D.M., Becker, R., Bulatov, V.J., 2004. On the evolution of crystallographic dislocation density in non-homogeneously deforming crystals. J. Mech. Phys. Solids 52, 1213–1246.

Asaro, R.J., Suresh, S., 2005. Mechanistic models for the activation volume and rate sensitivity in metals with nanocrystalline grains and nano-scale twins. Acta Materialia 53, 3369–3382.

Asaro, R.J., Krysl, P., Kad, B., 2003. Deformation mechanism transition in nanoscale FCC metals. Philos. Mag. Lett. 83, 733–743.

Bachurin, D.V., Murzaev, R.T., Nazarov, A.A., 2003. Atomistic computer and disclination simulation of [0 0 1] tilt boundaries in nickel and copper. Fiz. Met. Metalloved. 96, 11–17.

Benkassem, S., Capolungo, L., Cherkaoui, M., 2007. Mechanical properties and multi-scale modeling of nanocrystalline materials. Acta Materialia 55, 3563–3572.

Berbenni, S., Favier, V., Lemoine, X., Berveiller, M., 2004. Micromechanical modeling of the elastic viscoplastic behavior of polycrystalline steels having different microstructures. Mater. Sci. Eng. A 372, 128–136.

Buehler, M.J., Hartmaier, A., Gao, H.J., 2003. Atomistic and continuum studies of crack-like diffusion wedges and associated dislocation mechanisms in thin films on substrates. J. Mech. Phys. Solids 51, 2105–2125.

Buehler, M.J., Hartmaier, A., Gao, H., 2004. Hierarchical multi-scale modeling of plasticity of submicron thin metal films. Modeling and Simulation Mater. Sci. Eng. 12, 391–413.

Cai, B., Kong, Q.P., Lu, L., Lu, K., 2000. Low temperature creep of nanocrystalline pure copper. Mater. Sci. Eng. A 286, 188–192.

Cai, B., Kong, Q.P., Cui, P., Lu, L., Lu, K., 2001. Creep behavior of cold-rolled nanocrystalline pure copper. Scr. Materialia 45, 1407–1413.

Capolungo, L., Cherkaoui, M., Qu, J., 2005a. A self consistent model for the inelastic deformation of nanocrystalline materials. J. Eng. Mater. Technol. 127, 400–407.

Capolungo, L., Jochum, C., Cherkaoui, M., Qu, J., 2005b. Homogenization method for strength and inelastic behavior of nanocrystalline materials. Int. J. Plasticity 21, 67–82.

Capolungo, L., Cherkaoui, M., Qu, J., 2007. On the elastic-viscoplastic behavior of nanocrystalline materials. Int. J. Plasticity 23, 561–591.

Coble, R.L., 1963. A model for boundary diffusion controlled creep in polycrystalline materials. J. Appli. Phys. 34, 1679–1682.

Derlet, P.M., Van Swygenhoven, H., 2002. Length scale effects in the simulation of deformation properties of nanocrystalline metals. Scr. Materialia 47, 719–724.

Dimiduk, D.M., Koslowski, M., LeSar, R., 2006. Preface to the viewpoint set on: statistical mechanics and coarse graining of dislocation behavior for continuum plasticity. Scr. Materialia 54, 701–704.

Froseth, A.G., Derlet, P.M., Van Swygenhoven, H., 2004. Dislocations emitted from nanocrystalline grain boundaries: Nucleation and splitting distance. Acta Materialia 52, 5863–5870.

Gutkin, M.Y., Ovid'Ko, I.A., Skiba, N.V., 2003. Transformation of grain boundaries due to disclination motion and emission of dislocations pairs. Mater. Sci. Eng. A 339, 73–80.

Hall, E.O., 1951. The deformation and aging of mild steel. Proc. Phys. Soc. London B 64, 747.

Haslam, A.J., Moldovan, D., Phillpot, S.R., Wolf., D., Gleiter, H., 2002. Combined atomistic and mesoscale simulation of grain growth in nanocrystalline thin films. Comput. Mater. Sci. 23, 15–32.

Hirth, J.P., Lothe, J., 1982. Theory of Dislocations. Wiley, New York.

Hirth, J.P., Pond, R.C., Lothe, J., 2006. Disconnections in tilt walls. Acta Materialia 54, 4237–4245.

Hosford, W.F., 1993. The Mechanics of Crystals and Textured Polycrystals. Oxford University Press, New York.

Jiang, B., Weng, G.J., 2004. A generalized self consistent polycrystal model for the yield strength of nanocrystalline materials. J. Mech. Phys. Solids 52, 1125–1149.

Ke, M., Hackney, S.A., Milligan, W.W., Aifantis, E.C., 1995. Observations and measurement of grain rotation and plastic strain in nanostructured metal thin films. Nanostructured Mater. 5, 689–697.

Kelchner, C.L., Plimpton, S.J., Hamilton, J.C., 1998. Dislocation nucleation and defect structure during surface indentation. Phys. Rev. B 58, 11085–11088.

Kim, B.-N., Hiraga, K., Morita, K., 2005. Viscous grain-boundary sliding and grain rotation accommodated by grain-boundary diffusion. Acta Materialia 53, 1791–1798.

Kim, H.S., Estrin, Y., 2005. Phase mixture modeling of the strain rate dependent mechanical behavior of nanostructured materials. Acta Materialia 53, 765–772.

Kim, H.S., Estrin, Y., Bush, M.B., 2000. Plastic deformation behaviour of fine grained materials. Acta Materialia 48, 493–504.

Kim, H.S., Estrin, Y., Bush, M.B., 2001. Constitutive modelling of strength and plasticity of nanocrystalline metallic materials. Mater. Sci. Eng. A 316, 195–199.

Kocks, U.F., Argon, A.S., Ashby, M.F., 1975. Thermodynamics and kinetics of slip. Prog. Mater. Sci. 19, 1–291.

Konstantinidis, D.A., Aifantis, E.C., 1998. On the "anomalous" hardness of nanocrystalline materials. Nanostructured Mater. 10, 1111–1118.

Kumar, K.S., Suresh, S., Chisolm, M.F., Horton, J.A., Wang, P., 2003. Deformation of electrodeposited nanocrystalline nickel. Acta Materialia 51, 387–405.

Kurtz, R.J., Hoagland, R.G., Hirth, J.P., 1999. Computer simulation of extrinsic grain-boundary defects in the sigma 11, $\langle 1\,0\,1\rangle$ $\{1\,3\,1\}$ symmetric tilt boundary. Philos. Mag. A (Phys. Conden. Matter: Structure, Defects Mech. Properties) 79, 683–703.

Lebensohn, R.A., Bringa, E.M., Caro, A., 2007. A viscoplastic micromechanical model for the yield strength of nanocrystalline materials. Acta Materialia 55, 261–271.

LeSar, R., Rickman, J.M., 2004. Incorporation of local structure in continuous theory of dislocations. Phys. Rev. B 69, 172105.

Li, J.C.M., 1963. Petch relation and grain boundary sources. Trans. Metall. Soc. AIME 227, 239.
Li, Y.J., Blum, W., Breutinger, F., 2004. Does nanocrystalline cu deform by coble creep near room temperature. Mater. Sci. Eng. A 387–389, 585–589.
Lu, H., Daphalapurkar, N.P., Wang, B., Roy, S., Komanduri, R., 2006. Multiscale simulation from atomistic to continuum—Coupling molecular dynamics (MD) with the material point method (MPM). Philos. Mag. 86, 2971–2994.
Lu, L., Schwainer, R., Shan, Z.W., Dao, M., Lu, K., Suresh, S., 2005. Nano-sized twins induce high rate sensitivity of flow stress in pure copper. Acta Materialia 53, 2169–2179.
Markmann, J., Bunzel, P., Rosner, H., Liu, K.W., Padmanabhan, K.A., Birringer, R., Gleiter, H., Weissmuller, J., 2003. Microstructure evolution during rolling of inert-gas condensed palladium. Scr. Materialia 49, 637–644.
Melchionna, S., Ciccotti, G., Holian, B.L., 1993. Hoover NPT dynamics for systems varying in shape and size. Mol. Phys. 78, 533–544.
Mishin, Y., Mehl, M.J., Papaconstantopoulos, D.A., Voter, A.F., Kress, J.D., 2001. Structural stability and lattice defects in copper: ab initio, tight-binding, and embedded-atom calculations. Phys. Rev. B 63, 224106–224111.
Muller, P., Saul, A., 2004. Elastic effects on surface physics. Surf. Sci. Rep. 54, 157.
Nozieres, P., Wolf, D.E., 1988. Interfacial properties of elastically strained materials. I. Thermodynamics of a planar interface. Z. Phy. B (Conden Matter) 70, 399.
Petch, N.J., 1953. The cleavage strength of polycrystals. J. Iron Steel Inst. 174, 25–28.
Randle, V., 1993. The Measurement of Grain Boundary Geometry. Institute of Physics Publishing, Bristol.
Rickman, J.M., LeSar, R., 2006. Issues in the coarse-graining of dislocation energetics and dynamics. Scr. Materialia 54, 735–739.
Rittner, J.D., Seidman, D.N., 1996. $\langle 1\,1\,0 \rangle$ symmetric tilt grain-boundary structures in FCC metals with low stacking-fault energies. Phys. Rev. B: Conden. Matter. 54, 6999.
Sanders, P.G., Eastman, J.A., Weertman, J.R., 1997a. Elastic and tensile behavior of nanocrystalline copper and palladium. Acta Materialia 45, 4019–4025.
Sanders, P.G., Rittner, M., Kiedaisch, E., Weertman, J.R., Kung, H., Lu, Y.C., 1997b. Creep of nanocrystalline Cu, Pd, and Al-Zr. Nanostructured Mater. 9, 433–440.
Sansoz, F., Molinari, J.F., 2005. Mechanical behavior of sigma tilt grain boundaries in nanoscale Cu and Al: a quasicontinuum study. Acta Materialia 53, 1931–1944.
Schuh, C.A., Nieh, T.G., Yamasaki, T., 2002. Hall–Petch breakdown manifested in abrasive wear resistance of nanocrystalline nickel. Scr. Materialia 46, 735–740.
Spearot, D.E., Jacob, K.I., McDowell, D.L., 2005. Nucleation of dislocations from [0 0 1] bicrystal interfaces in aluminum. Acta Materialia 53, 3579–3589.
Spearot, D.E., Jacob, K.I., McDowell, D.L., 2007. Dislocation nucleation from bicrystal interfaces with dissociated structure. Int. J. Plasticity 23, 143–160.
Sutton, A.P., Vitek, V., 1983. On the structure of tilt grain boundaries in cubic metals. I. Symmetrical tilt boundaries. Philos. Trans. R. Soc. London A 309, 1–36.
Van Swygenhoven, H., Caro, A., 1997. Plastic behavior of nanophase Ni: a molecular dynamics computer simulation. Appl. Phys. Lett. 71, 1652.
Van Swygenhoven, H., Derlet, P.M., Froseth, A.G., 2004. Stacking fault energies and slip in nanocrystalline metals. Nature Materials 3, 399–403.
Wang, Y.M., Ma, E., 2004. Strain hardening, strain rate sensitivity and ductility of nanostrcutured metals. Mater. Sci. Eng. A 375–377, 46–52.
Wang, Y.M., Hamza, A.V., Ma, E., 2005. Activation volume and density of mobile dislocations in plastically deforming nanocrystalline Ni. Appl. Phys. Let. 86, 241917.
Warner, D.H., Sansoz, F., Molinari, J.F., 2006. Atomistic based continuum investigation of plastic deformation in nanocrystalline copper. Int. J. Plasticity 22, 754.
Wei, Y.J., Anand, L., 2004. Grain-boundary sliding and separation in polycrystalline metals: application to nanocrystalline FCC metals. J. Mech. Phys. Solids 52, 2587.
Wolf, D.E., Nozieres, P., 1988. Interfacial properties of elastically strained materials. II. Mechanical and melting equilibrium of a curved interface. Z. Phys. B (Conden. Matter) 70, 507.
Wolf, D., Yamakov, Y., Phillpot, S.R., Mukherjee, A.K., 2003. Deformation mechanism and inverse Hall–Petch behavior in nanocrystalline materials. Z. Metall. 94, 1052–1061.
Yamakov, V., Wolf, D., Salazar, M., Phillpot, S.R., Gleiter, H., 2001. Length-scale effects in the nucleation of extended dislocations in nanocrystalline al by molecular-dynamics simulation. Acta Materialia 49, 2713–2722.

Yamakov, V., Wolf, D., Phillpot, S.R., Gleiter, H., 2002. Grain boundary diffusion creep in nanocrystalline palladium by molecular dynamics simulation. Acta Materialia 50, 61–73.

Yamakov, V., Wolf, D., Phillpot, S.R., Mukherjee, A.K., Gleiter, H., 2003. Deformation mechanism crossover and mechanical behaviour in nanocrystalline materials. Philos. Mag. Lett. 83, 385–393.

Yin, W.M., Whang, S.H., Mirshams, R., Xiao, C.H., 2001. Creep Behavior of Nanocrystalline Nickel at 290 and 373 K, Vol. A301. Elsevier, Cincinatti, OH, USA (p. 18).

Zhu, Y.T., Langdon, T.G., 2005. Influence of grain size on deformation mechanisms: An extension to nanocrystalline materials. Mater. Sci. Eng. A 409, 234–242.